

The endogenous caspase-8 inhibitor c-FLIP_L regulates ER morphology and crosstalk with mitochondria

ES Marini¹, C Giampietri¹, S Petrungraro¹, S Conti¹, A Filippini¹, L Scorrano^{2,3,4,5} and E Ziparo^{*1,4,5}

Components of the death receptor-mediated pathways like caspase-8 have been identified in complexes at intracellular membranes to spatially restrict the processing of local targets. In this study, we report that the long isoform of the cellular FLICE-inhibitory protein (c-FLIP_L), a well-known inhibitor of the extrinsic cell death initiator caspase-8, localizes at the endoplasmic reticulum (ER) and mitochondria-associated membranes (MAMs). ER morphology was disrupted and ER Ca²⁺-release as well as ER-mitochondria tethering was decreased in c-FLIP^{-/-} mouse embryonic fibroblasts (MEFs). Mechanistically, c-FLIP ablation resulted in enhanced basal caspase-8 activation and in caspase-mediated processing of the ER-shaping protein reticulon-4 (RTN4) that was corrected by re-introduction of c-FLIP_L and caspase inhibition, resulting in the recovery of a normal ER morphology and ER-mitochondria juxtaposition. Thus, the caspase-8 inhibitor c-FLIP_L emerges as a component of the MAMs signaling platforms, where caspases appear to regulate ER morphology and ER-mitochondria crosstalk by impinging on ER-shaping proteins like the RTN4.

Cell Death and Differentiation (2015) 22, 1131–1143; doi:10.1038/cdd.2014.197; published online 12 December 2014

Cellular FLICE inhibitory proteins (c-FLIP) inhibit death receptor (DR)-mediated apoptosis, by preventing caspase-8 activation.¹ Among the three identified c-FLIP splicing forms,^{2,3} c-FLIP_{S,R} were described as cytosolic, whereas c-FLIP_L was also observed in the nucleus. A pool of membrane-bound c-FLIP_L was also described⁴ suggesting that caspase-8/c-FLIP_L could re-distribute on stimulation, leading to a more subtle regulation of caspase-8 activity depending on substrates localization.⁵ Furthermore, caspase-8 itself and Fas-Associated Death Domain adaptor protein (FADD) were found or were shown to re-localize in local complexes on ER^{6–8} and mitochondria,^{9,10} mediating the exchange of signals between the two organelles.^{11–13} Several molecular platforms containing both membrane-bound proteins and cytosolic apoptosis modulators have been identified at the ER-mitochondria interface (the so-called mitochondria-associated membranes or MAMs),¹⁴ controlling ER-mitochondria anchorage as well as lipid metabolism, Ca²⁺ signaling and apoptosis.¹⁵ MAMs have been recently described as lipid raft-like domains that orient proteins to promote the ER-mitochondria juxtaposition;¹⁶ consequently, alterations in their composition may profoundly affect the physical and functional inter-organelle crosstalk. Furthermore, as mitochondrial and ER membranes are continuously and concertedly remodeled,¹⁷ it is not surprising that membrane-

shaping proteins can also exert a function in regulating the ER-mitochondria coupling.^{12,18} Different families of ER-shaping proteins control the organization of peripheral ER, which consists of sheet-like cisternae and tubules connected by three-way junctions.¹⁹ Among these, Reticulons (RTN) and Deleted in Polyposis locus 1 (DP1) proteins cause the ER membrane to curve and tubulate,^{20,21} whereas the GTPases Atlantins (ATL) promote the branching of ER tubules;²² finally, ER sheet-enriched proteins such as the 63-kDa cytoskeleton-linking membrane protein (CLIMP63) control the width of ER cisternae, anchoring the organelle to microtubules and maintaining its spatial distribution.^{23,24} Along with other components of the extrinsic apoptosis, here we described for the first time the enrichment of c-FLIP_L at ER and ER-mitochondria interface. Furthermore, we observed that ER structure and tethering to mitochondria are impaired in cells lacking c-FLIP. Given the importance of membrane-shaping proteins and MAM complexes in regulating organelles structure and ER-mitochondria juxtaposition, we focused on the mechanism underlying this phenotype and we found that c-FLIP_L deficiency induces the caspase-mediated processing of RTN4, thus affecting organelle shape and coupling to mitochondria. We therefore concluded that c-FLIP_L is a novel regulator of ER morphology and ER-mitochondria crosstalk.

¹Istituto Pasteur-Fondazione Cenci Bolognetti, DAHFMO – Section of Histology and Medical Embryology, Sapienza University of Rome, Rome, Italy; ²Department of Biology, University of Padua, Padua, Italy and ³Dulbecco-Telethon Institute, Venetian Institute of Molecular Medicine, Padua, Italy

*Corresponding author: E Ziparo, DAHFMO—Histology and Medical Embryology, Sapienza University of Rome, Via Antonio Scarpa 16, Rome 00161, Italy. Tel: +39 0649766586; Fax: +39 064462854; E-mail: elio.ziparo@uniroma1.it

⁴These authors contributed equally to this work.

⁵Co-corresponding authors.

Abbreviations: ATL, atlastin; BAP31, B-cell associated protein 31; BAPTA, 1,2-Bis(2-aminophenoxy)ethane-N,N,N',N'-tetraacetic acid tetrakis(acetoxymethyl ester); Bid, BH3-interacting domain death agonist; c-FLIP, cellular FLICE inhibitory protein; CLIMP63, cytoskeleton-associated protein 4; DP1, deleted in polyposis locus 1; ERYFP, ER-targeted yellow fluorescent protein; FADD, Fas-associated death domain adaptor protein; IP₃, inositol 1,4,5-trisphosphate; MAMs, mitochondria-associated membranes; mtRFP, mitochondria-targeted red fluorescent protein; PARP, poly-(ADP-ribose) polymerase; RTN4, reticulon-4; STS, staurosporine; TG, thapsigargin; WT, wild type

Received 18.3.14; revised 11.9.14; accepted 27.10.14; Edited by M Piacentini; published online 12.12.14

Results

c-FLIP_L localizes at ER and MAMs. We investigated c-FLIP subcellular localization by performing cell fractionation and indirect immunofluorescence. Percoll-purified fractions from the mouse liver, devoid of cross-contaminations as indicated by western blotting (WB) analysis of specific markers (Figure 1a), were assayed. In agreement with previous evidence,^{25,26} c-FLIP_S was found in the cytosol (Figure 1b). Conversely, c-FLIP_L localized also at the ER+LM (Light Membranes) and MAMs fractions (Figure 1b). The pattern of distribution of calnexin (CNX)²⁷ and AKT,²⁸ both previously identified at MAMs, further substantiated the specificity of c-FLIP_L subcellular localization (Figures 1a and b). In homogenates from mouse embryonic fibroblasts (MEFs),

c-FLIP_L was similarly retrieved in both ER+LM and crude mitochondria still containing ER and MAMs as contaminants (Figure 1c). Confocal analysis corroborated c-FLIP distribution in MEFs. In the left panel of Figure 1d, yellow discrete areas represented the ER-mitochondria contact points. A similar pattern of co-localization was observed for c-FLIP and mitochondria (Figure 1d, central panel), whereas a wider overlapping was reported between the ER-protein calreticulin (CRT) and c-FLIP (Figure 1d, right panel), confirming c-FLIP distribution at the ER and ER-mitochondria contacts points. According to biochemical and morphological evidence, we concluded that ER and MAMs contain c-FLIP_L, which is conversely absent from mitochondria devoid of the interacting ER.

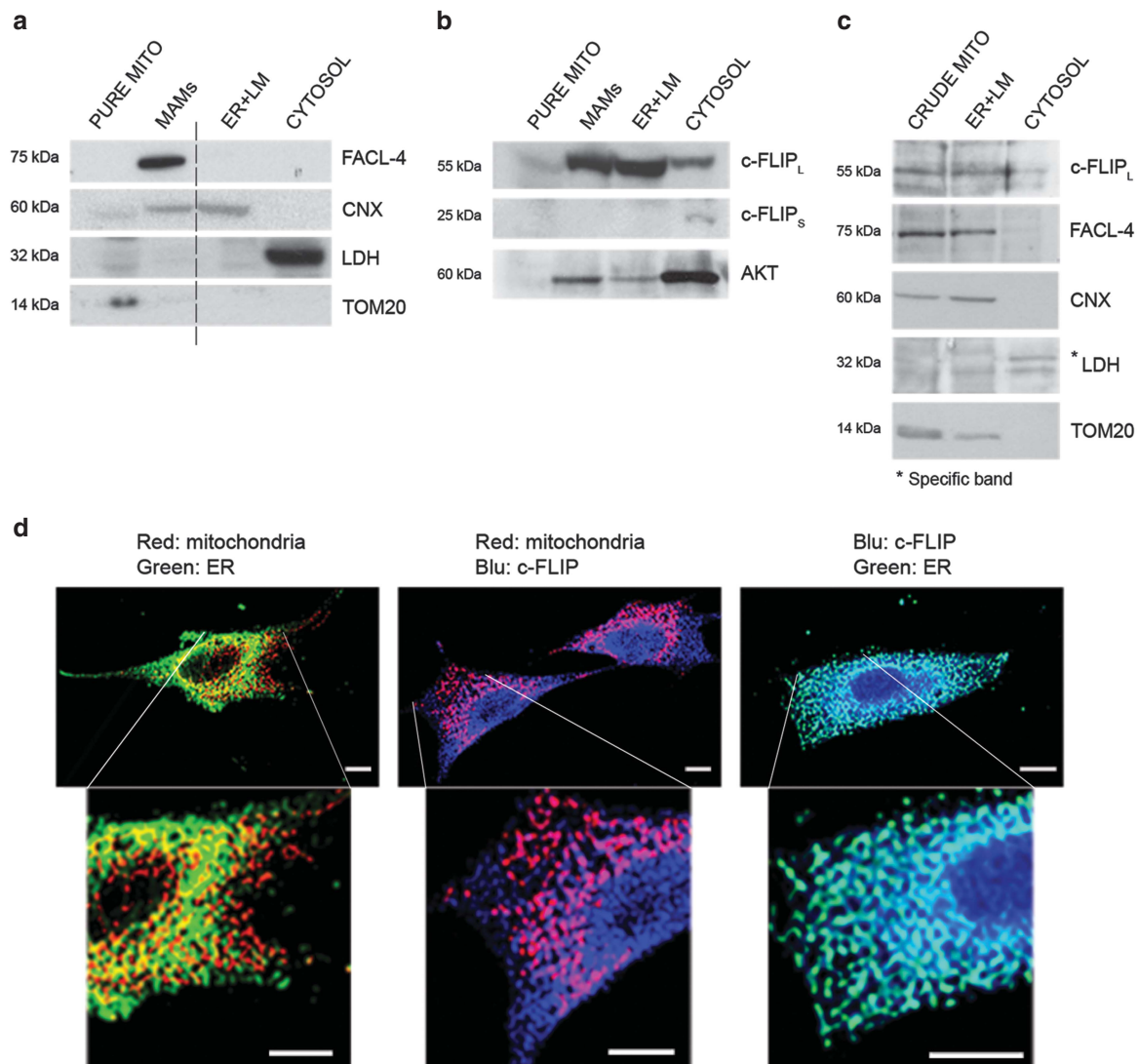


Figure 1 c-FLIP_L is retrieved at ER and MAMs. (a, b) Proteins (20 μg) from Percoll-purified subcellular fractions of the mouse liver were separated by SDS-PAGE and immunoblotted with the indicated antibodies, specific for each fraction. The translocase of the mitochondrial outer membrane 20 (TOM20) was used as marker for mitochondria, the lactate dehydrogenase (LDH) as marker for cytosolic fraction. Calnexin (CNX) is considered as a marker of both ER and MAMs, whereas the long-chain fatty-acid CoA synthases (FACL4) is MAM-enriched. Distant parts from the same gel were joined at dashed lines. (c) Subcellular fractions and immunoblot analysis from WT MEFs. (d) Immunofluorescence and confocal analysis of endogenous c-FLIP subcellular localization. WT MEFs were transfected with pDsRed2-mito encoding for the mitochondrial-targeted fluorescent protein (mtRFP) to label mitochondria and immunostained for the endogenous ER marker calreticulin (CRT) and for c-FLIP. Left and central panels indicate co-localization of ER with mitochondria, and of mitochondria with c-FLIP. Right panel indicates co-localization of ER and c-FLIP. Boxes denote magnified areas. Scale bar, 20 μm

Lack of c-FLIP_L controls ER integrity and ER-mitochondria tethering. The subcellular distribution of c-FLIP_L prompted us to investigate its involvement in the regulation of ER morphology and tethering to mitochondria. To this aim, WT and c-FLIP^{-/-} MEFs²⁹ transfected with mitochondria- and ER-targeted fluorescent proteins (respectively mtRFP and ERYFP) were used, and ER and mitochondrial morphology was investigated by comparing three-dimensional (3D) reconstructions of volume-rendered confocal stacks of mtRFP and ERYFP. c-FLIP depletion did not significantly alter mitochondrial morphology or distribution (Figure 2a). Conversely, whereas WT cells showed a well-organized network of interconnected tubules spanning the whole cytosol (Figure 2b, left panel), c-FLIP^{-/-} cells displayed a deranged ER, characterized by fragmented and enlarged cisternae, seemingly to the detriment of reticular ER at the cell periphery (Figure 2b, central panel). Such defects were partially restored on c-FLIP_L re-introduction in ablated MEFs (Figure 2b, right panel). To ensure that ER defects were not a result of transfections toxicity, immunofluorescence analysis of the endogenous ER-protein CRT (Figure 2c) and electron microscopy (EM) analysis were performed (Figure 2d), confirming the enlargement of ER cisternae in c-FLIP^{-/-} cells with respect to the tubular ER in WT MEFs. Fluorescence recovery after photobleaching (FRAP) of ERYFP was finally used to quantitatively assess the ER integrity, as the speed with which fluorescence returns to the photobleached region is dependent on the degree of ER luminal contiguity.³⁰ In accordance with morphological evidence, FRAP analysis further substantiated ER impairment and lack of integrity at the cell periphery of c-FLIP^{-/-} cells (Figure 2e), which were partially restored by c-FLIP_L re-introduction, hence corroborating c-FLIP role in this phenotype. Confirming the ER fragmentation mainly at the cell periphery, no major differences in ER luminal contiguity were observed in the perinuclear area (Figure 2f). In view of c-FLIP_L localization at MAMs and of its involvement in ER shape, we investigated whether c-FLIP could have a role also in ER-mitochondria tethering. To address this point, we firstly measured the ability of crude mitochondria from WT and c-FLIP^{-/-} MEFs to interact with microsomal components as CNX. As shown in Figure 2g, crude mitochondria from ablated MEFs were less contaminated by microsomes than those isolated from WT, indicating diminished ER-mitochondria interactions. Successively, we measured the ER-mitochondria distance by semi-quantitative confocal microscopy analysis of volume-rendered 3D reconstructions of z-axis stacks of confocal images of ERYFP and mtRFP.^{17,18} Whereas WT MEFs showed several yellow areas of co-localization, representing the ER-mitochondria contact points, c-FLIP^{-/-} cells revealed lower ER-mitochondria juxtaposition (Figure 2h), which was partially restored on c-FLIP_L re-introduction. Quantitatively, Manders' colocalization coefficient³¹ confirmed these evidence, revealing ~15% reduction in the ER-to-mitochondria tethering in c-FLIP^{-/-} MEFs, that was counterbalanced by c-FLIP_L re-expression (Figure 2i). The occurrence of inter-organelle contacts in WT and c-FLIP^{-/-} MEFs was also verified by EM analysis (Figure 2d).

ER-shaping protein Reticulon-4 is reduced in c-FLIP ablated cells. Defective ER morphology indicated that c-FLIP_L could have a role in maintaining the ER structure. To characterize the molecular mechanism involved, we first compared the expression levels of different ER proteins to discern whether ER expansion could be related to excessive ER membrane proliferation. However, we did not detect significant differences between WT and c-FLIP^{-/-} cells in any of the tested ER-resident proteins (Figure 3a). We further compared MFN2 levels, as its involvement in ER-mitochondria tethering and morphology was previously reported.¹⁸ However, we did not notice major differences either in MFN2 levels between WT and c-FLIP^{-/-} MEFs, or in c-FLIP_L between WT and MFN2^{-/-} cells, suggesting a MFN2-independent mechanism (Figure 3b). As aberrant ER enlargement observed in c-FLIP^{-/-} cells was similar to ER defects associated with RTN4 depletion,²⁰ or to overexpression of ATLS³² or CLIMP63,²³ we compared the expression levels of these ER-shaping proteins in microsomal fractions from WT and c-FLIP^{-/-} MEFs (Figures 3c and e). Interestingly, c-FLIP-depleted cells displayed diminished expression of RTN-4A,B_{2,1} isoforms (Figure 3c), whereas no significant variations were observed in CLIMP63 or in ATLS_{1,2} (Figures 3d and e). Only a slight, but not statistically significant, reduction in ATLS₃ was noticed (Figure 3e), indicating the involvement of RTN4 in ER alterations affecting c-FLIP^{-/-} MEFs. Total lysates from the two cell lines, besides evidencing the differences in RTN-4A,B_{2,1}, also revealed additional lower-molecular weight bands, compatible with cleaved fragments of this protein and visible predominantly in ablated MEFs (Figure 3f). Conversely, no extra bands of CLIMP63 were observed (Figure 3g); therefore, proposing that cleavage events could affect the RTN4 integrity in c-FLIP^{-/-} MEFs, in turn the disrupted ER morphology.

TNF α induces RTN4 processing. Previous evidence indicated that caspases and their inhibitors could impinge on levels of endogenous ER morphogenic proteins. In particular, caspase-7 was reported to mediate the cleavage of RTN-4B.³³ Owing to the ability of c-FLIP to control the apical caspase-8, which activates the caspase-7, we investigated whether increased caspase activation has occurred in cells lacking c-FLIP, in turn accounting for RTN4 processing. In agreement with this hypothesis, the basal caspase-8 activity was enhanced in c-FLIP^{-/-} MEFs (Figure 4a). Successively, to better characterize the involvement of caspase-8/c-FLIP axis and extrinsic apoptotic response in RTN4 cleavage and ER alterations, we exposed c-FLIP^{-/-} cells to increasing doses of TNF α , known to strongly induce the extrinsic pathway of apoptosis through caspase activation.²⁹ As shown, we observed a rapid, but defective cleavage of RTN4 (Figure 4b, upper panel: RTN-4A; lower panel: RTN-4B_{2,1}), decreasing at higher doses of TNF α despite the dose-dependent increase in caspase-8 activity (Figure 4c) and cleavage of caspase-3 and poly-(ADP-ribose) polymerase (PARP) (Figure 4d), which suggested an efficient activation of caspase-mediated pathways. As non-neural cells as MEFs abundantly express RTN-4B_{2,1} as compared with the little amount of RTN-4A, evaluation of RTN-4B_{2,1} was chosen for the following experiments. As reduction of RTN-4B_{2,1}

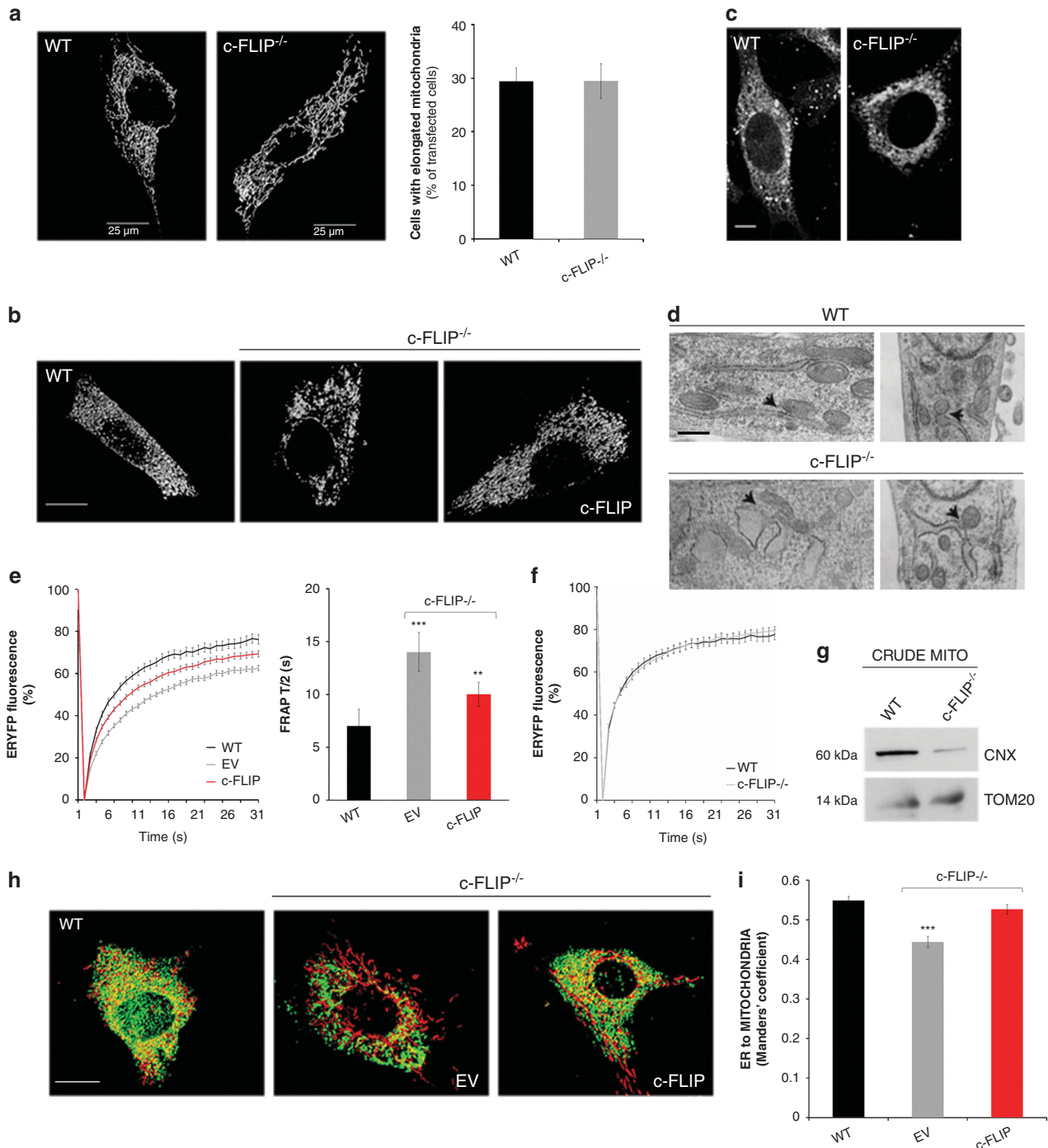


Figure 2 c-FLIP_L depletion affects ER morphology and tethering to mitochondria. **(a) Left:** Representative 3D-reconstructions of mitochondria in MEFs of the indicated genotype transfected with mtRFP. **Right:** mean \pm S.E.M. ($n = 4$, 25 cells per experiment) of data from **a**. **(b)** Representative 3D-reconstructions of ER in MEFs of the indicated genotype co-transfected with ERYFP and with plasmids encoding for c-FLIP_L or for the empty vector. 'c-FLIP' indicates c-FLIP_L re-introduction in depleted MEF. Scale bar, 25 μ m. **(c)** Immunofluorescence analysis of the resident ER protein CRT in WT and c-FLIP^{-/-} MEFs. **(d)** Representative EM images of ER and ER-mitochondria contact points in WT and c-FLIP^{-/-} cells. Scale bar, 0.54 μ m in the upper, right panel; 0.35 μ m in other panels. Arrows indicate ER-mitochondria proximity. **(e, f)** Fluorescence recordings from real-time sequence of ERYFP FRAP in c-FLIP^{-/-} and WT MEFs at the cell periphery (**e**) and in the perinuclear region (**f**). The histogram reported mean \pm S.E.M. ($n = 5$, 10 cells per experiment) of data from **e** (** $P \leq 0.001$; *** $P \leq 0.0001$). In **e, f**, 16- μ m² regions were photobleached for a total of 3 s, using 100% laser power of the 488 nm line. The post-bleaching images were taken for a total of 120 s. 'c-FLIP' indicates c-FLIP_L re-introduction in depleted MEF, 'EV' the empty vector. **(g)** WB of the indicated proteins in crude mitochondrial fractions (20 μ g) from WT and c-FLIP^{-/-} MEFs. **(h)** Representative 3D-reconstructions of ER and mitochondria in MEFs of the indicated genotype co-transfected with mtRFP, ERYFP and the reported plasmids. Yellow areas indicate that organelles are closer than 270 nm. Scale bar, 25 μ m. **(i)** Mean \pm S.E.M. ($n = 5$, 10 cells per experiment) of interaction data from **h** (** $P \leq 0.001$).

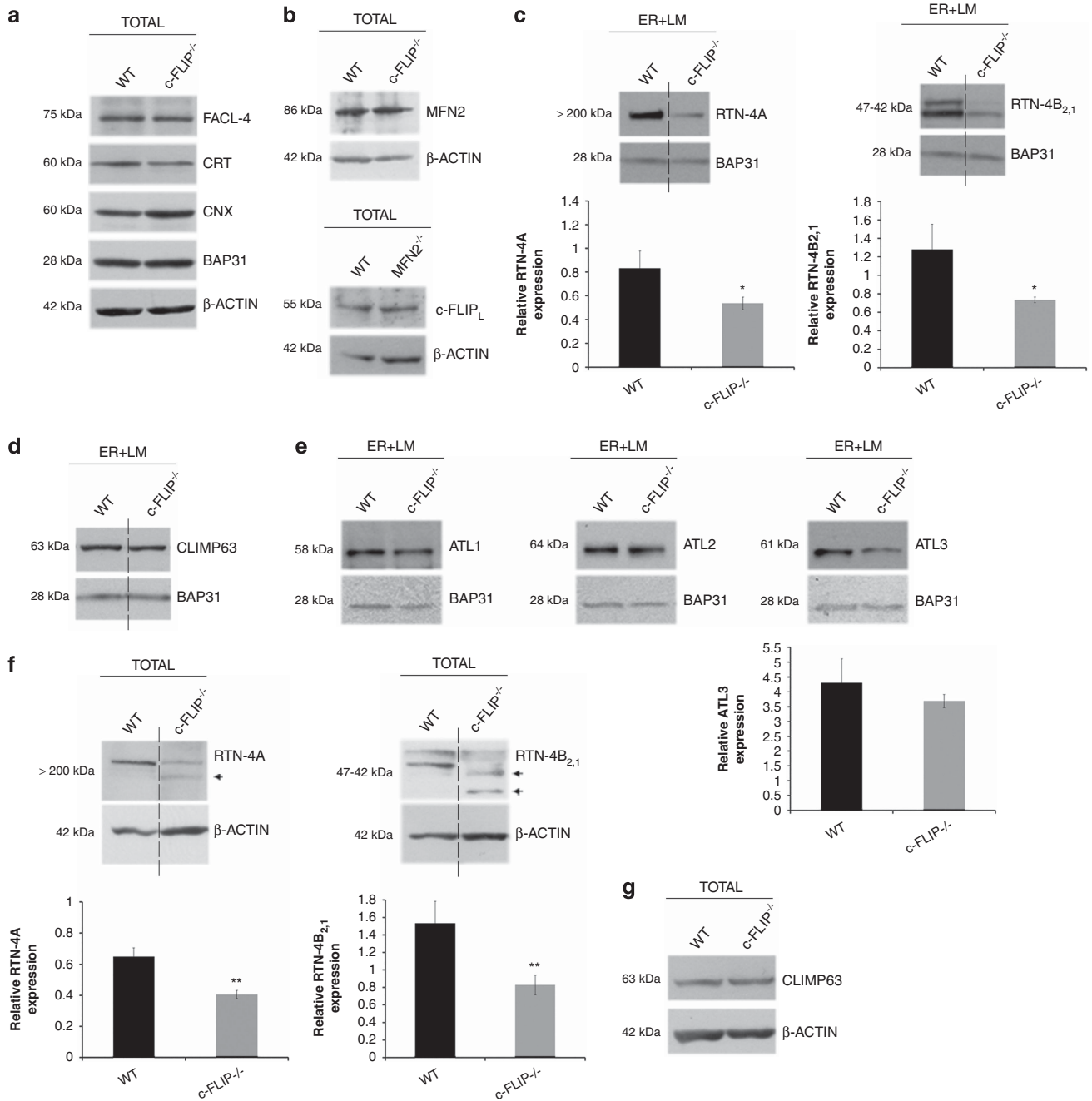


Figure 3 Evaluation of different ER markers in WT and c-FLIP-ablated cells. (a) Total lysates (50 μ g) from WT and c-FLIP^{-/-} MEFs were separated by SDS-PAGE and immunoblotted for different ER markers. (b) **Upper panel:** representative WB analysis of MFN2 level in total lysates from WT and c-FLIP^{-/-} MEFs ($n=4$). **Lower panel:** representative WB analysis of c-FLIP_L level in total lysates from WT and MFN2^{-/-} MEFs ($n=3$). (c, d) Representative WB analysis of expression levels of RTN-4A and -B_{2,1} (c) and CLIMP63 (d) in ER fractions isolated from WT and c-FLIP^{-/-} MEFs. The same amount of proteins was used and protein loading was controlled by evaluating the expression of the ER-resident protein BAP31. Histograms indicate the mean \pm S.E.M. of full length, ER+LM-associated RTNs densitometric analysis ($n=3$ for RTN-4A; $n=3$ for RTN-4B_{2,1}). (e) WB analysis of expression levels of ATL1,2,3 in ER fractions. BAP31 was used as loading control. The densitometric analysis reported in the histogram, represented the mean \pm S.E.M. ($n=3$) of ATL3 level. (f, g) WB analysis of RTN-4A, B_{2,1} (f) and CLIMP63 (g) levels in total lysates from c-FLIP^{-/-} and WT MEFs. Histograms indicate the mean \pm S.E.M. of full-length RTN densitometric analysis ($n=3$ for RTN-4A; $n=6$ for RTN-4B_{2,1}). In c, d, f broken lines indicate where a lane was deleted

cleavage at increasing TNF α doses (Figure 4b) or at longer time points (Figures 4e and f) occurred concomitantly to the formation of a higher-weight form of RTN-4B_{2,1} (indicated by the asterisk in the less-exposed lane) compatible with the phosphorylated form of the protein, we hypothesized that in our model RTN-4B_{2,1} processing could be prevented by an

unidentified TNF α -induced phosphorylation event. Interestingly, cyclin-dependent kinases 1/2 (CDK1/2)-mediated phosphorylation of RTN-4B was reported to negatively control RTN4 processing.³³ In accordance with our hypothesis, co-treatment of c-FLIP^{-/-} MEFs with TNF α and the CDK1/2 pharmacological inhibitor JNJ-7706621 lowered the

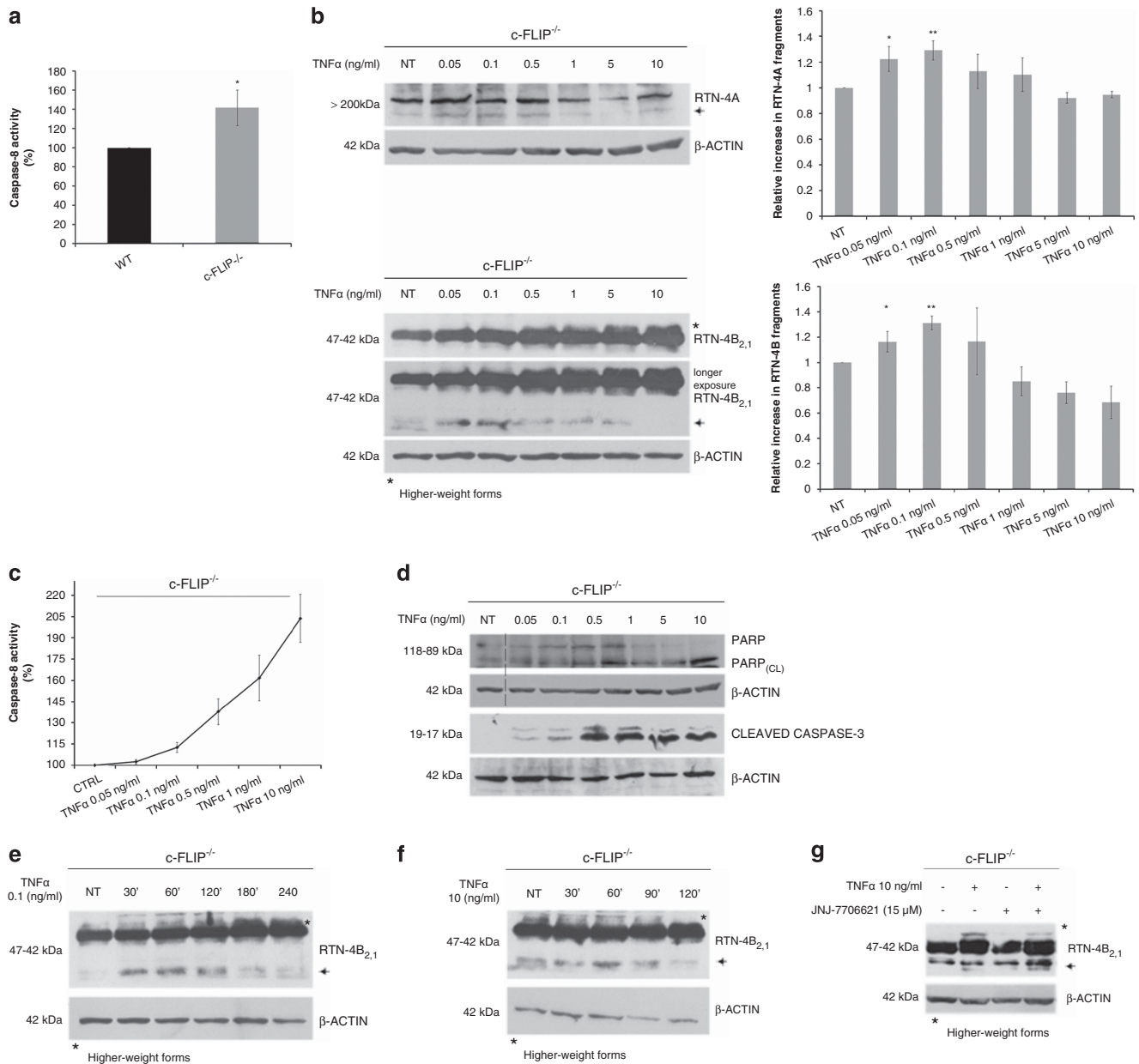


Figure 4 Caspase activation impacts on RTN4 levels in c-FLIP^{-/-} MEFs. **(a)** Basal caspase-8 activity was measured in c-FLIP^{-/-} and WT MEFs. Mean ± S.E.M. ($n = 7$) ($*P \leq 0.05$). **(b)** Evaluation of RTN-4A and -B_{2,1} cleavage by WB analysis in c-FLIP^{-/-} MEFs treated for 2 h with the indicated doses of TNF α . Histograms indicate the mean ± S.E.M. of RTN4 fragments densitometric analysis ($n = 3$ for RTN-4A in the upper panel; $n = 3$ for RTN-4B_{2,1} in the lower panel). **(c)** Colorimetric evaluation of caspase-8 activity on treatment of c-FLIP^{-/-} cells with the indicated doses of TNF α . **(d)** WB analysis of caspase-3 and PARP cleavage in c-FLIP^{-/-} MEFs treated with the indicated doses of TNF α . **(e, f)** Representative WB analysis of RTN-4B_{2,1} cleavage in c-FLIP^{-/-} MEFs treated, respectively, with TNF α 0,1 ng/ml **(e)** and 10 ng/ml **(f)** at the indicated time points. In **b, d-f**, β -actin was used to normalize. **(g)** Evaluation of RTN-4B_{2,1} cleavage by WB analysis in c-FLIP^{-/-} MEFs treated with TNF α 10 ng/ml alone or in combination with JNJ-7706621 15 μ M

accumulation of the higher-weight form of RTN-4B_{2,1} and increased the formation of cleavage fragments with respect to c-FLIP^{-/-} cells treated with TNF α alone (Figure 4g). We also observed mild RTN-4B_{2,1} cleavage in WT cells on TNF α treatment. Such cleavage increased when TNF α was combined with the *de novo* protein synthesis inhibitor cycloheximide (data not shown). Together our data highlight a role for TNF α -induced caspase activation in RTN4 cleavage, in c-FLIP-deficient cells as well as in their WT counterpart.

A caspase-mediated pathway is involved in RTN4 alterations and influences ER morphology and tethering to mitochondria. As already reported in other experimental models,^{34,35} we verified that c-FLIP ablation in MEFs enhanced the basal caspase-8 activity (Figure 4a), which was restored by both the specific caspase-8 inhibitor zIETD and c-FLIP_L re-introduction (Figure 5a). To confirm the involvement of caspases in TNF α -mediated RTN4 processing in c-FLIP^{-/-} cells, zIETD and the pan-caspases inhibitors zVAD were used. Although both inhibitors were efficient in

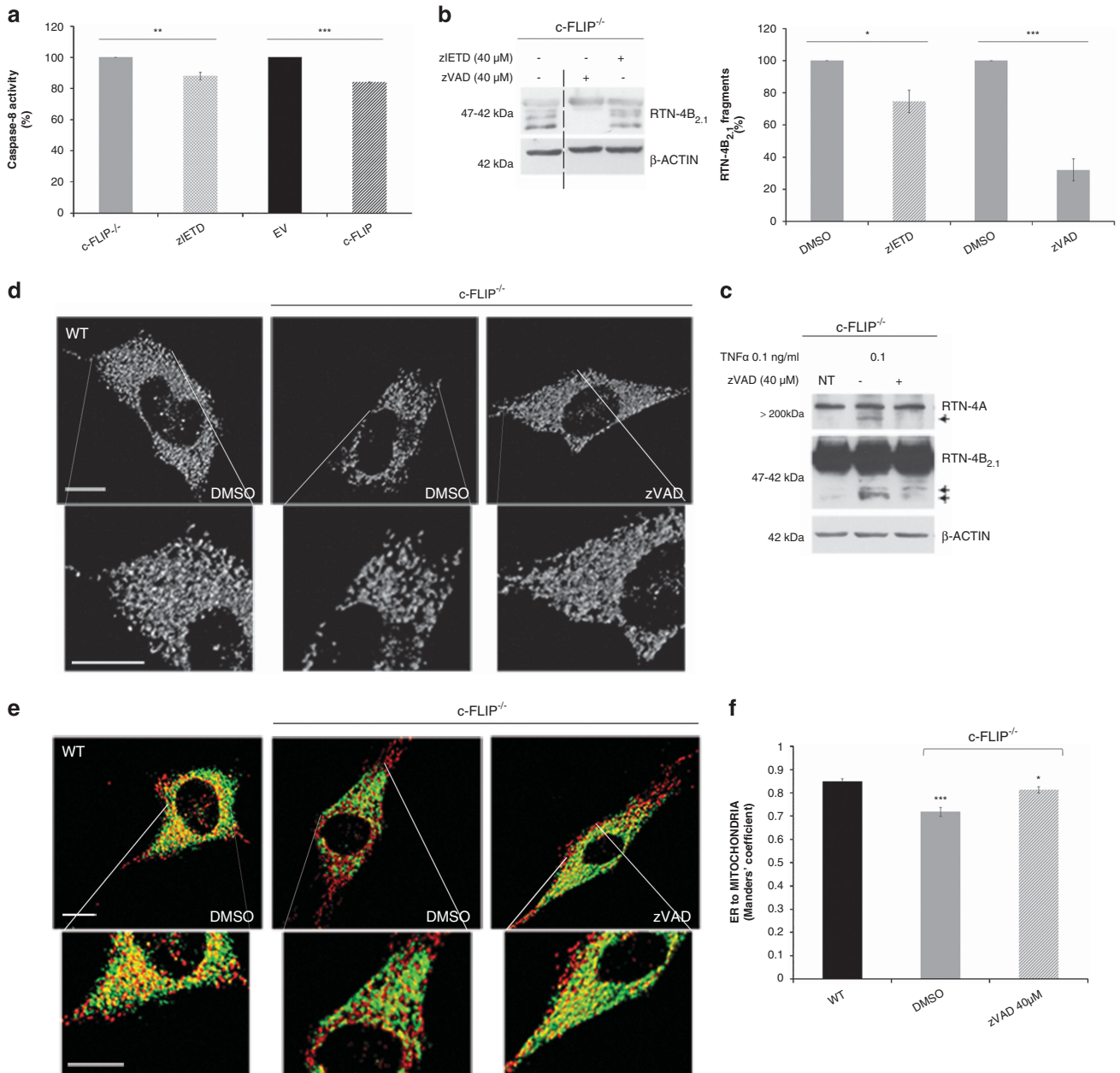


Figure 5 Caspase-inhibition rescues RTN4 processing and ameliorates ER morphology and tethering to mitochondria. **(a)** Caspase-8 activity was measured in c-FLIP^{-/-} MEFs on caspase-8 inhibition with zIETD and c-FLIP_L re-introduction. Mean ± S.E.M. ($n = 3$ experiments) (** $P \leq 0.001$; *** $P \leq 0.0001$). **(b)** WB evaluation of basal RTN4 cleavage, on pharmacological caspase inhibition with zIETD or zVAD. Broken lines indicate that we joined together distant parts from the same gel. The histogram represents the mean ± S.E.M. of RTN-4B_{2.1} fragments densitometric analysis ($n = 3$). **(c)** WB analysis of RTN4 fragments formation in c-FLIP^{-/-} cells on treatment with the indicated dose of TNF α , alone or in combination with the inhibitor zVAD. **(d)** Representative 3D-reconstructions of ER in MEFs of the indicated genotype transfected with ERYFP, and treated with DMSO or zVAD (40 μ M). Scale bar, 20 μ m. **(e)** Representative 3D-reconstructions of ER and mitochondria in MEFs of the indicated genotype co-transfected with mtRFP, ERYFP and treated with DMSO or zVAD (40 μ M). Scale bar, 20 μ m. **(f)** Mean ± S.E.M. ($n = 5$, 10 cells per experiment) of interaction data from **e** (*** $P \leq 0.0001$). In **b**, **c** β -actin was used to normalize

reducing the basal RTN4 proteolysis, even though to a different extent (Figure 5b), zVAD efficaciously diminished also the TNF α -induced RTN-4B_{2.1} processing (Figure 5c). This evidence further corroborated the role of caspases and components of DR-mediated pathway in controlling the RTN4 cleavage. In view of the essential role of reticulons in ER tubulogenesis, as well as of the involvement of caspases in RTN4 regulation, we wondered whether the altered ER

morphology of c-FLIP^{-/-} cells could be associated with the caspase-dependent RTN4 cleavage. To test this hypothesis, ER morphology and ER-mitochondria tethering of c-FLIP^{-/-} MEFs pre-treated with zVAD were compared with those of WT and c-FLIP^{-/-} cells exposed to the vehicle DMSO. Strengthening the proposed model, semi-quantitative confocal microscopy analysis of volume-rendered 3D reconstructions of z-axis stacks of confocal images of WT and c-FLIP^{-/-}

cells transfected with ERYFP revealed that caspase-inhibition was sufficient to rescue the ER morphology of c-FLIP^{-/-} MEFs (Figure 5d). Moreover, as estimated by measuring the quantitative Manders' co-localization coefficient, zVAD was also efficient in restoring the ER-mitochondria distance of c-FLIP^{-/-} MEFs to levels comparable to those of WT (Figure 5e and f), hence underlying the potential role of caspases in regulating membrane-localized proteins and ER-mitochondria interactions.

c-FLIP ablation results in disturbed Ca²⁺ signaling. Integrity of ER and ER-mitochondria contact points have been demonstrated to be crucial for Ca²⁺ signaling.³⁶ In view of the role of c-FLIP_L at the ER and MAMs, we investigated its involvement in Ca²⁺ exchange between the two organelles. We firstly compared the increase in cytosolic Ca²⁺ concentration ([Ca²⁺]_c) in Fura-2AM-loaded WT and c-FLIP^{-/-} MEFs on treatment with the sarcoplasmic-endoplasmic reticulum Ca²⁺ ATPase (SERCA) inhibitor thapsigargin (TG), causing the passive ER discharge, and with ATP which induces ER Ca²⁺ release from inositol 1,4,5-trisphosphate (IP₃)-sensitive stores. EGTA was added to all solutions to assess only intracellular calcium fluxes. c-FLIP^{-/-} MEFs displayed severely blunted ER Ca²⁺ release in response to both TG and ATP (Figures 6a and b). In addition, as [Ca²⁺]_c is buffered by mitochondria, along with the blunted ER Ca²⁺ release, in Rhod-2AM loaded c-FLIP^{-/-} cells also the mitochondrial Ca²⁺ peak evoked by ATP was significantly lower than that in WT (Figure 6c). Nevertheless, such defects were not restored by c-FLIP_L re-introduction, as we did not observe any amelioration in either ER Ca²⁺ release (Figure 6d) or mitochondrial Ca²⁺ entry (Figure 6e) in c-FLIP^{-/-} cells re-expressing c-FLIP_L with respect to c-FLIP^{-/-} MEFs transfected with the EV. According to our data, c-FLIP^{-/-} MEFs displayed reduced ER-mitochondria juxtaposition and diminished Ca²⁺ exchange. We therefore wondered whether the reduced ability of ER and mitochondria to exchange signals and calcium could impact on Ca²⁺-mediated apoptosis. In agreement with this hypothesis, cells lacking c-FLIP were more resistant than WT to hydrogen peroxide (H₂O₂), which is known to induce a Ca²⁺-dependent apoptotic response (Figure 6f).³⁷ Conversely, c-FLIP^{-/-} MEFs were as susceptible as WT to staurosporine (STS), which activates the mitochondrial pathway, but much more sensitive to DR-stimulation induced by TNF α , as previously reported (Figure 6g). Altogether our data demonstrate that c-FLIP ablation loosens ER-mitochondria juxtaposition, lowering Ca²⁺ transfer to mitochondria and impacting on sensitivity to Ca²⁺-dependent apoptosis.

Calcium chelation in WT MEFs induces ER changes. TG-induced ER Ca²⁺ release is an indirect measure of ER Ca²⁺ content at the steady state. According to our data suggesting diminished Ca²⁺ levels and Ca²⁺ exchange in cells lacking c-FLIP, we speculated that these differences could directly contribute to the observed ER defects. We therefore tested whether the chelator of free, cytosolic calcium 1,2-Bis(2-aminophenoxy)ethane-N,N,N',N'-tetraacetic acid tetrakis (acetoxymethyl ester) (BAPTA-AM) could modify the overall ER structure in WT and c-FLIP^{-/-} MEF. Unexpectedly,

BAPTA-AM affected ER shape and RTN-4B_{1,2} integrity of the two cell lines. These effects were more evident in WT MEFs (Figure 7a, left panels), leading to ER enlargement and fragmentation and resembling ER defects of c-FLIP^{-/-} MEFs, which were only marginally affected by Ca²⁺ chelation (Figure 7a, right panels). WB analysis further revealed that BAPTA-AM caused RTN-4B^{1,2} processing in WT cells, augmenting fragments formation in also c-FLIP^{-/-} cells. Despite these effects, BAPTA-AM did not modulate c-FLIP_L levels in WT cells, nor induced PARP cleavage (Figure 7b), suggesting a caspase-independent mechanism. Concordantly, whereas zVAD efficaciously diminished the basal RTN-4B_{1,2} cleavage in c-FLIP^{-/-} MEFs (Figure 7c), it did not abrogate the BAPTA-AM-induced RTN4 processing in either of the two cell lines (respectively, in Figures 7c and d). These data suggest that, in c-FLIP^{-/-} cells, ER effects and RTN4 processing could be also directly associated with disturbed calcium levels, besides to the caspase-dependent pathway.

Discussion

Components of DR signaling as caspase-8 have been identified on ER and mitochondria, suggesting that target specificity may depend on cellular compartments.⁵ In this study, we report that a fraction of the caspase-8 inhibitor c-FLIP_L is enriched at the ER and MAMs. Along with other MAM-proteins, whose ablation affects ER and mitochondrial morphology or their coupling,^{18,37,38} here we demonstrate that c-FLIP deficiency in MEFs impacts on ER organization, causing enlargement of ER sheets to the detriment of tubular structures. The relative amount of the ER-shaping proteins RTN/DP1 and CLIMP63 was described to influence the cell-type-specific ratio of sheets to tubules in mammalian cells.³⁹ Jozsef *et al.*⁴⁰ demonstrated that RTN4 deficiency in MEFs is sufficient to convert ER tubules to cisternal structures, without affecting other ER-shaping factors or ER-resident proteins.⁴⁰ Interestingly, we found decreased expression of RTN-4A,B_{2,1} in c-FLIP^{-/-} MEFs, whereas no major differences were observed in other ER-shaping proteins or in ER proteins, confirming that ER defects of c-FLIP^{-/-} MEFs were not related to variations in the overall ER content or to excessive CLIMP63 expression or ATL-mediated fusion.³² As caspase-7 was formerly reported to process the RTN-4B on its cytoplasmic tail on apoptotic induction,³³ we hypothesized that ER defects observed in c-FLIP^{-/-} cells could be associated with a deregulated, caspase-dependent processing of RTN4 occurring in cells lacking the inhibitor of caspase-8. In agreement with our hypothesis, here we demonstrate that c-FLIP^{-/-} MEFs show an increased basal RTN4 processing, and that TNF α is sufficient to accelerate its cleavage. Interestingly, despite TNF α promptly induced a dose-dependent activation of caspase-8 and caspase-3, we observed only an initial cleavage of RTN4, decreasing at higher doses of TNF α or at longer time points, concomitantly to the accumulation of a higher-weight form of RTN-4B_{2,1}. As Cyclin-dependent kinases 1/2 (CDK1/2) phosphorylate RTN4, abrogating its cleavage and inducing the accumulation of a higher-weight phosphorylated form, we hypothesized that the incomplete RTN4 processing could be associated with a CDK-mediated phosphorylation event. In accordance with

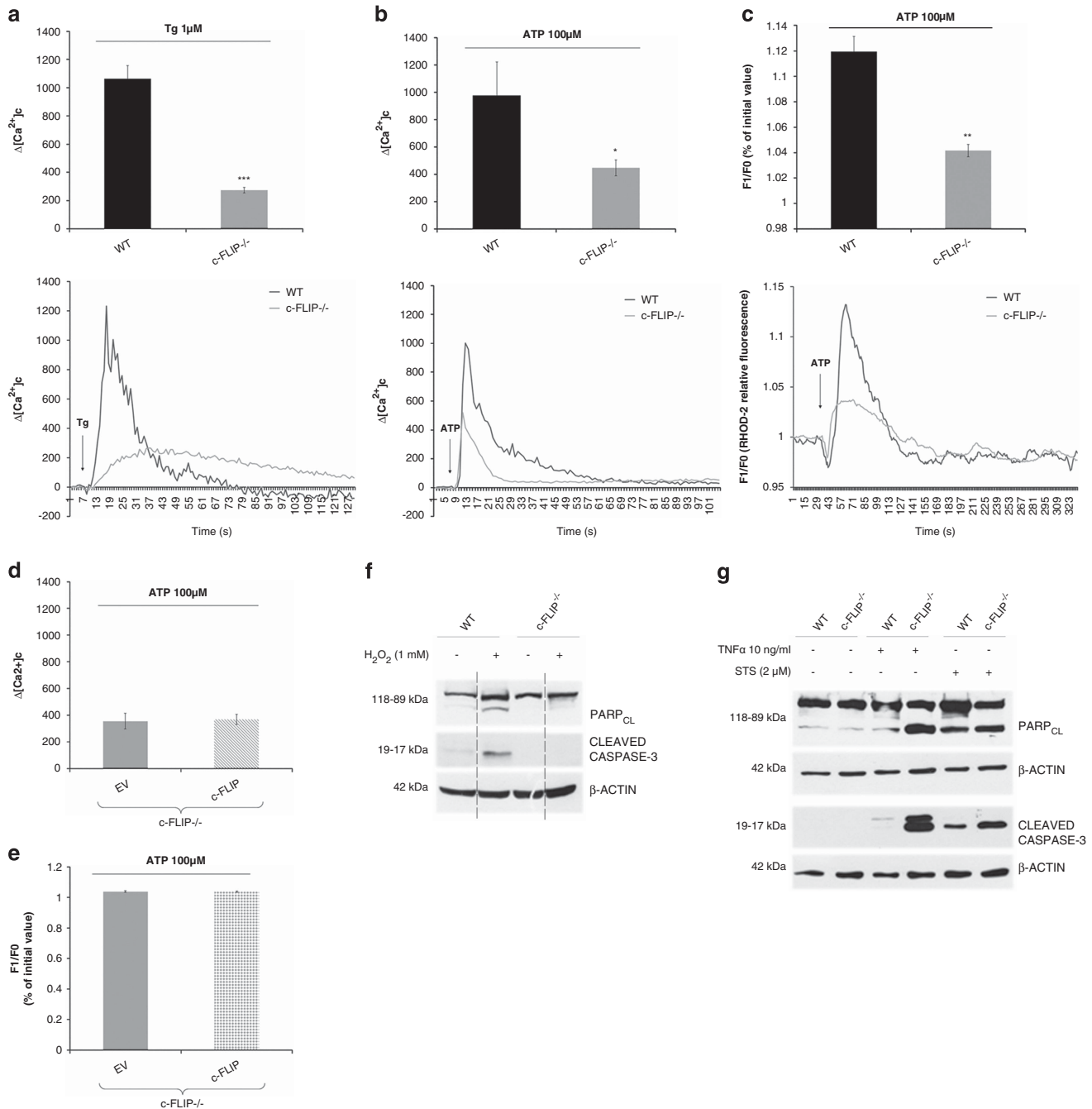


Figure 6 c-FLIP absence alters Ca²⁺ homeostasis and Ca²⁺-dependent apoptosis. **(a)** Fura-2AM recordings of cytosolic Ca²⁺ ([Ca²⁺]_c) after passive discharge of ER Ca²⁺ stores induced by 1 μ M TG in MEFs of the indicated genotype. **Upper panel:** maximum Ca²⁺ concentrations in bar charts. Mean \pm S.E.M. of $n=70-100$ cells. **Lower panel:** changes in Ca²⁺ concentrations shown as representative traces. **(b)** Fura-2AM recordings of cytosolic Ca²⁺ ([Ca²⁺]_c) after active ER Ca²⁺ release induced by 100 mM ATP in MEFs of the indicated genotype. **Upper panel:** maximum Ca²⁺ concentrations in bar charts. Mean \pm S.E.M. of $n=70-100$ cells. **Lower panel:** changes in Ca²⁺ concentrations shown as representative traces. **(c)** Rhod-2AM recordings of mitochondrial Ca²⁺ entry (F₁/F₀) after active ER-to-cytosol Ca²⁺ release induced by 100 mM ATP in MEFs of the indicated genotype. **Upper panel:** maximum Ca²⁺ concentrations in bar charts. Mean \pm S.E.M. of $n=70-100$ cells. **Lower panel:** changes in Ca²⁺ concentrations. In **a-c** * $P \leq 0.05$; ** $P \leq 0.001$; *** $P \leq 0.0001$. **(d)** Fura-2AM recordings of cytosolic Ca²⁺ ([Ca²⁺]_c) after active ER Ca²⁺ release induced by 100 mM ATP in c-FLIP^{-/-} MEFs transfected with the indicated plasmids. **(e)** Rhod-2AM recordings of mitochondrial Ca²⁺ entry (F₁/F₀) after active ER-to-cytosol Ca²⁺ release induced by 100 mM ATP in c-FLIP^{-/-} MEFs transfected with the indicated plasmids. **(f)** Representative WB analysis of total lysates (40 μ g) from MEFs of the indicated genotype, on treatment with H₂O₂ 1 mM for 3 h. Apoptosis was investigated evaluating cleavage of PARP and caspase-3. **(g)** Representative WB analysis of total lysates (40 μ g) from MEFs of the indicated genotype, on treatment with STS (2 μ M) for 3h and TNF α 10 ng/ml for 2 h. Apoptosis was investigated evaluating cleavage of PARP and caspase-3. ($n=5$ for H₂O₂ treatment; $n=3$ for STS and TNF α treatments)

and worsened RTN-4B_{2,1} fragmentation in c-FLIP^{-/-} MEFs. These effects were more pronounced in WT than in c-FLIP^{-/-} cells, probably as a consequence of the different Ca²⁺ content of the two cell lines. To better investigate whether modulation of Ca²⁺ levels could modify the ER organization independently of c-FLIP and caspases, we evaluated c-FLIP_L levels and PARP cleavage as a measure of caspase activation. Interestingly, BAPTA-AM neither modulated c-FLIP_L in WT MEFs, nor induced RTN-4B_{2,1} cleavage via caspases. Nevertheless, although caspase activation was not described as necessary to ER remodeling during apoptosis,⁴¹ we cannot exclude that the increased caspase-8 activity observed in c-FLIP^{-/-} cells at basal conditions could impinge on RTN4 cleavage and ER integrity, in turn emphasizing the role of caspase-mediated processing of RTN4. To summarize, in addition to showing c-FLIP_L at the ER and MAMs, in this paper we demonstrate its relevance in modulating ER morphology and tethering to mitochondria. We also provide evidence of a new role for caspases in ER structure modulation via processing of RTN4. Although the importance of RTNs transmembrane domains in ER tubulation was firstly described,^{20,21} modifications in the intrinsically unstructured, cytosolic regions of RTN4⁴² have been reported to influence the variable functions of RTNs or specific interactions.^{20,40} We can therefore speculate that caspases, acting on exposed regions of RTN4, might disturb the localization⁴³ or the ability of ER-shaping proteins to form complexes and interact with cytoskeletal components or organelles.⁴⁴ Concluding, the present study highlights additional non-apoptotic roles for the death-receptor pathway, a frame in which c-FLIP_L and caspases emerge as new factors in the maintenance of ER homeostasis.

Materials and Methods

Cell cultures and reagents. Wild type (WT) and c-FLIP^{-/-} MEFs were a generous gift of Tak W. Mak (Amgen Institute, Toronto, Canada). MEFs were cultured in DMEM, enriched with 10% fetal bovine serum, glutamine (2 mmol/l), sodium pyruvate (1 mmol/l) and non-essential amino acids, in the presence of penicillin (100 U/ml) and streptomycin (100 µg/ml). The Inhibition Caspase-8 inhibitor II, indicated as Z-IE(OMe)TD(OMe)-FMK (zIETD), was purchased from Calbiochem (San Diego, CA, USA). Cells were treated for 24 h with zIETD 40 µM or with the vehicle DMSO. The *N*-Benzyloxycarbonyl-Val-Ala-Asp(O-Me) fluoromethyl ketone (zVAD-FMK) was purchased from Sigma-Aldrich (St Louis, MO, USA). Cells were treated for 24 h with zVAD 40 µM or with the vehicle DMSO. Where indicated, JNJ-7706621 was added to cell cultures. After 1 h pre-treatment, TNF α was added. JNJ-7706621 was synthesized by the Cancer Therapeutics Research Team (Johnson & Johnson Pharmaceutical Research and Development, LLC). Transfections with pDsRed2-Mito (Clontech laboratories INC—Palo Alto, CA, USA), pEGFP-ER (Clontech) and pBluescript or c-FLIP_L plasmid (kindly provided by M. Peter (The Ben May Institute for Cancer Research, University of Chicago, Chicago, IL USA) were performed using Transfectin reagent (BioRad, Hercules, CA, USA) at 2 µg/µl, or Lipofectamin Reagent (Invitrogen, San Giuliano Milanese, Italy) at 4 µg/µl, according to the manufacturer's instructions. Where indicated, BAPTA-AM (Sigma-Aldrich) 5 µM or the vehicle DMSO was added to cell cultures for 3 h at 37 °C and ER morphology and WB analysis of RTN4 were performed.

Subcellular fractionation. Whole mouse liver from adult CD1 mice or WT and c-FLIP^{-/-} MEFs obtained from four, confluent, 500 cm² petri dishes was washed twice with PBS, re-suspended in isolation buffer (IB, 200 mM sucrose, 1 mM EGTA-Tris, and 10 mM Tris-MOPS, pH 7.4), and then broken up by dounce homogenization. Purified fractions were obtained according to Frezza *et al.*⁴⁵ Protein concentration was determined by micro BCA assay (Pierce Rockford, USA) and 20 µg of protein extract was separated by SDS-PAGE and immunoblotted for the indicated antibodies. All animal procedures were conducted in compliance with the Italian Ministry for Health guidelines.

Immunoblotting. Cells were collected and lysed in lysis buffer (Cell Signaling Technology, Danvers, MA, USA) in the presence of complete protease-inhibitor mixture (Sigma-Aldrich). Protein concentration was determined by micro BCA assay (Pierce, Rockford, IL, USA) and the indicated proteins were separated by SDS-PAGE and transferred onto polyvinylidene difluoride (PVDF, BioRad) or nitrocellulose membranes (Amersham Bioscience, Piscataway, NJ, USA). Membranes were probed using the following antibodies: anti- β -actin (1:10 000, Sigma-Aldrich); anti-calnexin (1:2000, Abcam, Cambridge, UK); anti-Tom20 (1:10000, Santa Cruz Biotechnology, Santa Cruz, CA, USA); anti-lactate dehydrogenase (LDH) (1:2000, Rockland); anti-long-chain fatty-acid CoA synthases (FACL4) (1:500, Santa Cruz Biotechnology); anti-calreticulin (CRT) (1:1000, Abcam); anti-c-FLIP Dave II clone (1:800, Alexis, Lausen, Switzerland); anti-RTN4 (1:1000, Abcam); anti-CLIMP63 (1:1000, Proteintech Group, Chicago, IL, USA); anti-cleaved caspase-3 (1:500, Cell Signaling Technology) and anti-PARP (1:1000; Cell Signaling Technology).

Imaging. For confocal imaging and analysis of the morphology and tethering of ER and mitochondria, cells seeded on 24-mm round glass coverslips and incubated in Hanks balanced salt solution (HBSS), supplemented with Hepes 10 mM, were placed on the stage of a Nikon Eclipse TE300 inverted microscope equipped with a spinning-disk PerkinElmer Ultraview LCI confocal system, a piezoelectric z-axis motorized stage (Pifoc, Physik Instrumente, Germany) and an Orca ER 12-bit charge-coupled device camera (Hamamatsu Photonics, Japan). Cells expressing ERYFP and/or mRFP were excited using the 488 nm or the 543 nm line of the HeNe laser (PerkinElmer, Waltham, MA, USA) by using a \times 60 1.4 NA Plan Apo objective (Nikon Corporation, Japan). For confocal z-axis stacks, images separated by 0.2 µm along the z-axis were acquired. To evaluate ER morphology and ER-mitochondria tethering on zVAD or BAPTA treatment a Leica confocal microscope (Laser Scanning TCS SP2, Leica Microsystems Heidelberg GmbH, Mannheim, Germany) equipped with Ar/ArKr and He/Ne lasers and with a \times 40 oil 1.40 plan Apo immersion objective was utilized. Analysis of the interactions between ER and mitochondria was performed with the software ImageJ. Deconvolution, 2D- and 3D-reconstruction and surface rendering were realized using the VolumeJ plugin of ImageJ. Analysis of the interaction between ER and mitochondria was performed using Manders' colocalization coefficient.³¹

Fluorescence recovery after photobleaching. Cells were plated and transfected with ERYFP as previously described. After 48 h they were incubated in HBSS and placed on the stage of a laser scanning microscope (TCS SP5, Leica). Using the LasAF software (Leica), 16-µm² regions were manually defined to be bleached. To bleach the YFP fluorescence, one z-plane was bleached for a total of 3 s using 100% laser power of the 514 nm laser line with a \times 63, 1.4NA objective. The post-bleaching images were taken at 0.937 s intervals for a total of 120 s. Intensities of the photobleached regions were measured and normalized to the intensities of the same region before photobleaching.

Ratiometric measurement of cytosolic Ca²⁺ concentration. A total of 15 \times 10⁴ WT and c-FLIP^{-/-} MEFs were seeded on 35 mm Petri dishes. Twenty-four hours after seeding, cells were incubated for 45 min at 37 °C in culture medium containing Fura-2AM 3.5 µM (Invitrogen), which is a ratiometric fluorescent dye binding to free intracellular calcium. Cells were then washed free of Fura-2AM and Hanks balanced solution (HBSS, 130 mM NaCl, 5.2 mM KCl, 1 mM MgCl₂, 10 mM glucose, 10 mM HEPES, pH 7.4) was added. EGTA was added to all solutions. Dishes were placed into a culture chamber at 37 °C on the stage of an inverted fluorescence microscope (Nikon TE2000E) and connected to a cooled CCD camera (512B Cascade; Roper Scientific, Princeton Instruments, Trenton, NJ, USA). Samples were illuminated alternately at 340 and 380 nm using a random access monochromator (Photon Technology International, Birmingham, NJ, USA) and emission was detected using a 510 nm emission filter. Images were acquired (1-ratio image/s) using Metafluor software (Universal Imaging Corporation, Downingtown, PA, USA). Calibration was obtained at the end of each experiment by maximally increasing intracellular Ca²⁺-dependent Fura-2AM fluorescence with ionomycin salt solution (Sigma-Aldrich) 5 µM, followed by recording minimal fluorescence in a Ca²⁺-free medium. Ca²⁺ concentration was calculated according to the previously described formulas.⁴⁶ Where indicated, c-FLIP^{-/-} cells were transiently transfected with pBluescript or c-FLIP_L plasmids and ER-to-cytosol Ca²⁺-fluxes were measured in Fura-2AM-loaded cells.

Measurement of mitochondrial Ca²⁺ concentration. A total of 15 × 10⁴ WT and c-FLIP^{-/-} MEFs were seeded on 35 mm, high, glass bottom Petri dishes. Twenty-four hours after seeding, cells were incubated for 1 h at 37 °C in culture medium containing Rhod2-AM 6 μM (Invitrogen). The ester forms of this calcium indicator are cationic, resulting in potential-driven uptake into mitochondria. Cells were then washed with standard medium and EGTA-containing HBSS at room temperature. Single-cell fluorescence was excited at 545 nm using a random access monochromator (Photon Technology International) and emission was detected using a 580 nm emission filter. Images of the emitted fluorescence, obtained with a ×60 oil objective, were collected using Metafluor software (Universal Imaging Corporation). Where indicated, c-FLIP^{-/-} cells were transiently transfected with pBluescript or c-FLIP_L plasmids and mitochondrial Ca²⁺ entry were measured in Rhod-2AM-loaded cells.

Evaluation of caspase-8 activity. Caspase-8 activity was measured by the previously tested⁴⁷ colorimetric FLICE/Caspase-8 Assay kit (BioVision/Vinci-Biochem, Firenze, Italy) according to the manufacturer's protocol. Levels of caspase-8 activation were normalized by total protein concentration.

Transmission electron microscopy. For ultrastructural observation, cell monolayers were fixed in 2.5% glutaraldehyde (Electron Microscopy Science, Pennsylvania, USA) and in 0.1% cacodylate buffer (Electron Microscopy Science), postfixed in 1% osmium tetroxide (Electron Microscopy Science) and then treated with 1% tannic acid (Acros Organics, New Jersey, NJ, USA). Dehydrated in ethanol (Carlo Erba), cells were detached from the plastic dish by a brief treatment in 1% toluene (Carlo Erba). The pelleted monolayer was then incubated in a solution of 50% toluene and 50% EPON 812 (Electron Microscopy Science) and finally processed for conventional EPON 812 embedding. Ultra-thin sections were cut in a Leica Ultracut R ultramicrotome, contrasted for 10 min in 1% acid tannic and successively in 1% lead hydroxide (Società Italiana Chimici, Rome, Italy) and then viewed in a Hitachi 7000 transmission electron microscope.

Statistical analysis. Values are expressed as mean ± S.E. Statistical evaluation was performed by Student's *t*-test analysis and a value of *P* ≤ 0.05 was considered statistically significant.

Conflict of Interest

The authors declare no conflict of interest.

Acknowledgements. We thank Dr. Tak W. Mak for providing us with WT and c-FLIP^{-/-} MEFs, B. Esposito for her helpful insight of Ca²⁺ signaling, S. De Grossi for her support at the confocal microscope, members of Scorrano's lab, A. Favia and S. Palchetti for discussions and technical advice, and F. Palombi for her help with electron microscopy and advice in text preparation. This work was supported by PRIN 2010-2011 and Fondazione Roma grants to E. Ziparo and Telethon GGP12162 grant to L. Scorrano.

Author contributions

E.S.M. designed, performed experiments and wrote the paper, S.C. performed apoptosis experiments, C.G. and S.P. assisted in interpreting results and writing the manuscript, L.S. and E.Z. conceived the overall design and wrote the manuscript with input from A.F.

- Irmeler M, Thome M, Hahne M, Schneider P, Hofmann K, Steiner V *et al*. Inhibition of death receptor signals by cellular FLIP. *Nature* 1997; **388**: 190–195.
- Scaffidi C, Schmitz I, Kramer PH, Peter ME. The role of c-FLIP in modulation of CD95-induced apoptosis. *J Biol Chem* 1999; **274**: 1541–1548.
- Golks A, Brenner D, Fritsch C, Kramer PH, Lavrik IN. c-FLIP_R, a new regulator of death receptor-induced apoptosis. *J Biol Chem* 2005; **280**: 14507–14513.
- Shain KH, Landowski TH, Dalton WS. Adhesion-mediated intracellular redistribution of c-Fas-associated death domain-like IL-1-converting enzyme-like inhibitory protein-long confers resistance to CD95-induced apoptosis in hematopoietic cancer cell lines. *J Immunol* 2002; **168**: 2544–2553.
- Misra RS, Russell JQ, Koenig A, Hinshaw-Makepeace JA, Wen R, Wang D *et al*. Caspase-8 and c-FLIP_L associate in lipid rafts with NF-κB adaptors during T cell activation. *J Biol Chem* 2007; **282**: 19365–19374.
- Ng FW, Nguyen M, Kwan T, Branton PE, Nicholson DW, Cromlish JA *et al*. p28 Bap31, a Bcl-2/Bcl-X_L- and procaspase-8-associated protein in the endoplasmic reticulum. *J Cell Biol* 1997; **139**: 327–338.
- Breckenridge DG, Nguyen M, Kuppig S, Reth M, Shore GC. The procaspase-8 isoform, procaspase-8_L, recruited to the BAP31 complex at the endoplasmic reticulum. *Proc Natl Acad Sci USA*. 2002; **99**: 4331–4336.
- Xiang R, Liu Y, Zhu L, Dong W, Qi Y. Adaptor FADD is recruited by RTN3/HAP in ER-bound signaling complexes. *Apoptosis* 2006; **11**: 1923–1932.
- Gonzalez F, Schug ZT, Houtkooper RH, MacKenzie ED, Brooks DG, Wanders RJ *et al*. Cardiolipin provides an essential activating platform for caspase-8 on mitochondria. *J Cell Biol* 2008; **183**: 681–696.
- Schug ZT, Gonzalez F, Houtkooper RH, Vaz FM, Gottlieb E. BID is cleaved by caspase-8 within a native complex on the mitochondrial membrane. *Cell Death Differ* 2011; **18**: 538–548.
- Breckenridge DG, Stojanovic M, Marcellus RC, Shore GC. Caspase cleavage product of BAP31 induces mitochondrial fission through endoplasmic reticulum calcium signals, enhancing cytochrome c release to the cytosol. *J Cell Biol* 2003; **160**: 1115–1127.
- Simmen T, Aslan JE, Blagoveshchenskaya AD, Thomas L, Wan L, Xiang Y *et al*. PACS-2 controls endoplasmic reticulum-mitochondria communication and Bid-mediated apoptosis. *EMBO J* 2005; **24**: 717–729.
- Chandra D, Choy G, Deng X, Bhatia B, Daniel P, Tang DG. Association of active caspase 8 with the mitochondrial membrane during apoptosis: potential roles in cleaving BAP31 and caspase 3 and mediating mitochondrion-endoplasmic reticulum cross talk in etoposide-induced cell death. *Mol Cell Biol* 2004; **24**: 6592–6607.
- Vance JE. Phospholipid synthesis in a membrane fraction associated with mitochondria. *J Biol Chem* 1990; **265**: 7248–7256.
- de Brito OM, Scorrano L. An intimate liaison: spatial organization of the endoplasmic reticulum-mitochondria relationship. *EMBO J* 2010; **29**: 2715–2723.
- Area-Gomez E, Del Carmen Lara Castillo M, Tambini MD, Guardia-Laguarta C, de Groof AJ, Madra M *et al*. Upregulated function of mitochondria-associated ER membranes in Alzheimer disease. *EMBO J* 2012; **31**: 4106–4123.
- Rizzuto R, Pinton P, Carrington W, Fay FS, Fogarty KE, Lifshitz LM *et al*. Close contacts with the endoplasmic reticulum as determinants of mitochondrial Ca²⁺ responses. *Science* 1998; **280**: 1763–1766.
- de Brito OM, Scorrano L. Mitofusin 2 tethers endoplasmic reticulum to mitochondria. *Nature* 2008; **456**: 605–610.
- Friedman JR, Voeltz GK. The ER in 3D: a multifunctional dynamic membrane network. *Trends Cell Biol* 2011; **21**: 709–717.
- Voeltz GK, Prinz WA, Shibata Y, Rist JM, Rapoport TA. A class of membrane proteins shaping the tubular endoplasmic reticulum. *Cell* 2006; **124**: 573–586.
- Shibata Y, Voss C, Rist JM, Hu J, Rapoport TA, Prinz WA *et al*. The reticulon and DP1/Yop1p proteins form immobile oligomers in the tubular endoplasmic reticulum. *J Biol Chem* 2008; **283**: 18892–18904.
- Hu J, Shibata Y, Zhu PP, Voss C, Rismanchi N, Prinz WA *et al*. A class of dynamin-like GTPases involved in the generation of the tubular ER network. *Cell* 2009; **138**: 549–561.
- Shibata Y, Shemesh T, Prinz WA, Palazzo AF, Kozlov MM, Rapoport TA. Mechanisms determining the morphology of the peripheral ER. *Cell* 2010; **143**: 774–788.
- Nikonov AV, Hauri HP, Lauring B, Kreibich G. Climp-63-mediated binding of microtubules to the ER affects the lateral mobility of translocon complexes. *J Cell Sci* 2007; **120**: 2248–2258.
- Zhang J, Chen Y, Huang Q, Cheng W, Kang Y, Shu L *et al*. Nuclear localization of c-FLIP-L and its regulation of AP-1 activity. *Int J Biochem Cell Biol* 2009; **41**: 1678–1684.
- Katayama R, Ishioka T, Takada S, Takada R, Fujita N, Tsuruo T *et al*. Modulation of Wnt signaling by the nuclear localization of cellular FLIP-L. *J Cell Sci* 2010; **123**: 23–28.
- Myhill N, Lynes EM, Nanji JA, Blagoveshchenskaya AD, Fei H, Carmine Simmen K *et al*. The subcellular distribution of calnexin is mediated by PACS-2. *Mol Biol Cell* 2008; **19**: 2777–2788.
- Giorgi C, Ito K, Lin HK, Santangelo C, Wiecekowsky MR, Lebedzinska M *et al*. PML regulates apoptosis at endoplasmic reticulum by modulating calcium release. *Science* 2010; **330**: 1247–1251.
- Yeh WC, Itie A, Elia AJ, Ng M, Shu HB, Wakeham A *et al*. Requirement for Casper (c-FLIP) in regulation of death receptor-induced apoptosis and embryonic development. *Immunity* 2000; **12**: 633–642.
- Dayel MJ, Hom EF, Verkman AS. Diffusion of green fluorescent protein in the aqueous-phase lumen of endoplasmic reticulum. *Biophys J* 1999; **76**: 2843–2851.
- Manders EM, Verbeek FJ, Aten JA. Measurement of co-localisation of objects in dual-colour confocal images. *J Microscopy* 1993; **169**: 375–382.
- Orso G, Pendlin D, Liu S, Tosoletto J, Moss TJ, Faust JE *et al*. Homotypic fusion of ER membranes requires the dynamin-like GTPase atlastin. *Nature* 2009; **460**: 978–983.
- Schweigreiter R, Stasyk T, Contarini I, Frauscher S, Oertle T, Klimaschewski L *et al*. Phosphorylation-regulated cleavage of the reticulon protein Nogo-B by caspase-7 at a noncanonical recognition site. *Proteomics* 2007; **7**: 4457–4467.
- Day TW, Huang S, Safa AR. c-FLIP knockdown induces ligand-independent DR5-, FADD-, caspase-8-, and caspase-9-dependent apoptosis in breast cancer cells. *Biochem Pharmacol* 2008; **76**: 1694–1704.
- Wittkopf N, Gunther C, Martini E, He G, Amann K, He YW *et al*. Cellular FLICE-like inhibitory protein secures intestinal epithelial cell survival and immune homeostasis by regulating caspase-8. *Gastroenterology* 2013; **145**: 1369–1379.

36. Rizzuto R, Brini M, Murgia M, Pozzan T. Microdomains with high Ca²⁺ close to IP3-sensitive channels that are sensed by neighboring mitochondria. *Science* 1993; **262**: 744–747.
37. Cerqua C, Anesti V, Pyakurel A, Liu D, Naon D, Wiche G et al. Trichoplein/mitostatin regulates endoplasmic reticulum-mitochondria juxtaposition. *EMBO Rep* 2010; **11**: 854–860.
38. Zampese E, Fasolato C, Kipanyula MJ, Bortolozzi M, Pozzan T, Pizzo P, Presenilin 2 modulates endoplasmic reticulum (ER)-mitochondria interactions and Ca²⁺ cross-talk. *Proc Natl Acad Sci USA* 2011; **108**: 2777–2782.
39. Shibata Y, Hu J, Kozlov MM, Rapoport TA. Mechanisms shaping the membranes of cellular organelles. *Annu Rev Cell Dev Biol* 2009; **25**: 329–354.
40. Jozsef L, Tashiro K, Kuo A, Park E, Skoura A, Albinsson S et al. Ret1clun 4 is necessary for ER tubulation, STIM1-Orai1 coupling and store-operated calcium entry. *J Biol Chem* 2014; **289**: 9380–9395.
41. Ferrari D, Pinton P, Campanella M, Callegari MG, Pizzirani C, Rimessi A et al. Functional and structural alterations in the endoplasmic reticulum and mitochondria during apoptosis triggered by C2-ceramide and CD95/APO-1/FAS receptor stimulation. *Biochem Biophys Res Commun* 2010; **391**: 575–581.
42. Li M, Song J. The N- and C-termini of the human Nogo molecules are intrinsically unstructured: bioinformatics, CD, NMR characterization, and functional implications. *Proteins* 2007; **68**: 100–108.
43. Sparkes I, Tolley N, Aller I, Svozil J, Osterrieder A, Botchway S et al. Five Arabidopsis reticulon isoforms share endoplasmic reticulum location, topology, and membrane-shaping properties. *Plant Cell* 2010; **22**: 1333–1343.
44. Park SH, Zhu PP, Parker RL, Blackstone C. Hereditary spastic paraplegia proteins REEP1, spastin, and atlastin-1 coordinate microtubule interactions with the tubular ER network. *J Clin Invest* 2010; **120**: 1097–1110.
45. Frezza C, Cipolat S, Scorrano L. Organelle isolation: functional mitochondria from mouse liver, muscle and cultured fibroblasts. *Nat Protoc* 2007; **2**: 287–295.
46. Grynkiewicz G, Poenie M, Tsien RY. A new generation of Ca²⁺ indicators with greatly improved fluorescence properties. *J Biol Chem* 1985; **260**: 3440–3450.
47. Giampietri C, Petrunaro S, Padula F, D'Alessio A, Marini ES, Facchiano A et al. Autophagy modulators sensitize prostate epithelial cancer cell lines to TNF-alpha-dependent apoptosis. *Apoptosis* 2012; **17**: 1210–1222.



This work is licensed under a Creative Commons Attribution-NonCommercial-ShareAlike 3.0 Unported License. The images or other third party material in this article are included in the article's Creative Commons license, unless indicated otherwise in the credit line; if the material is not included under the Creative Commons license, users will need to obtain permission from the license holder to reproduce the material. To view a copy of this license, visit <http://creativecommons.org/licenses/by-nc-sa/3.0/>